Eur. Phys. J. D **42**, 435–440 (2007)
DOI: 10.1140/epjd/e2007-00051-7

THE EUROPEAN PHYSICAL JOURNAL D

Measurement of OH spatially resolved spectrum in a wire-plate pulsed streamer discharge

F. Liu, W. Wang[a], W. Zheng, and Y. Wang

State Key Laboratory of Materials Modification by Laser, Ion and Electron Beams, Dalian University of Technology, Dalian 116024, P.R. China

Received 1st October 2006 / Received in final form 28 January 2007
Published online 9 March 2007 –

Abstract. In this study, spatially resolved measurements of the emission intensity of OH ($A^2\Sigma \rightarrow X^2\Pi$, 0-0) and the vibrational temperature of N_2 (C) have been performed during a positive pulsed streamer discharge with a wire-plate electrode configuration at atmospheric pressure. The effects of pulse peak voltage, pulse repetition rate and the added O_2 flow rate on the spatial distributions of the emission intensity of OH ($A^2\Sigma \rightarrow X^2\Pi$, 0-0) and the vibrational temperatures of N_2 (C) perpendicular to the wire in the direction towards the plate (in the radial direction) are investigated. It has been found that the emission intensity of OH ($A^2\Sigma \rightarrow X^2\Pi$, 0-0) increases with increasing pulse peak voltage and pulse repetition rate and decreases with increasing the distance from the wire electrode. When the different oxygen flows are added in N_2 and H_2O mixture gas, the emission intensity of OH ($A^2\Sigma \rightarrow X^2\Pi$, 0-0) decreases with increasing the flow rate of oxygen. The vibrational temperature of N_2 (C) is nearly independent of pulsed peak voltage and pulsed repetition rate, but increases with increasing the added O_2 flow rate and keeps almost constant in the radial direction under the present experimental conditions. This measurement plays a crucial role in understanding the discharge characters of pulsed streamer discharge and establishing the molecule reaction dynamics model of pulsed streamer discharge.

PACS. 52.70.Kz Optical (ultraviolet, visible, infrared) measurements – 52.80.Hc Glow; corona – 82.33.Xj Plasma reactions (including flowing afterglow and electric discharges) – 52.20.Hv Atomic, molecular, ion, and heavy-particle collisions

1 Introduction

Pulsed streamer discharge is one of a few techniques that can produce non-thermal plasmas with a low gas temperature and a high-electron temperature at atmospheric pressure. Short-duration pulsed streamer discharge is more efficient in energy transfer than other non-thermal plasma techniques. Electrons obtain more energy compared to gas heating [1]. The chemically active species (OH, O, H, N, HO_2, N^+, N_2^+ and O_3 etc.) generated by electron collisions with ambient molecules in the pulsed streamer discharge are considered important in removal of acid gases from flue gases, organic compounds removal from water, bacterial decontamination, volatile organic compounds (VOCs) decomposition and destruction of other toxic compounds etc. fields [2–12]. Especially, OH radicals play the crucial role for their strong oxidation in many physicochemical processes [13–15].

In these physicochemical applications, chemically active species play the central role in the processes and therefore much attention has been devoted to the diagnosis investigation of those chemically active species and kinetics simulation study on the pulsed streamer discharge process [16–29]. Sun et al. [16] probed OH, O and H radicals generated by a pulsed corona discharge in water using optical emission spectroscopy. Tang et al. [17] present the diagnostic results of N^+ and N_2^+ produced by high-voltage pulsed corona discharge using a molecular beam mass spectrometer. Wang et al. [18–21] have analyzed the emission spectrum of OH, O and H produced in a needle-plate electrode system and OH in a wire-plate electrode configuration using positive pulsed corona discharge at atmospheric pressure. They also studied the radial profiles of high-energy electron density generated by a pulsed corona discharge in a wire-cylinder reactor using a pulsed corona discharge. Ono and Oda [22–25] had measured the density of OH radicals generated by a pulsed discharge with laser-induced fluorescence. They discussed the atomic O role in forming OH radicals and explored the formation and structure of primary and secondary streamers in the positive pulsed streamer discharge. Namihira et al. [26] determined the propagation velocity of pulsed streamer discharges in atmospheric air. Veldhuizen et al. [27] had studied the positive pulsed streamer propagation and branching. Eichwald et al. [28] developed

[a] e-mail: wangwenc@dlut.edu.cn

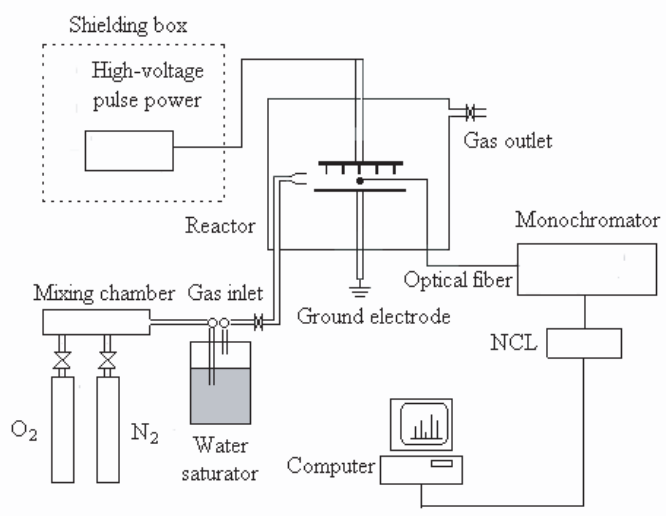

Fig. 1. Schematic of the experimental setup.

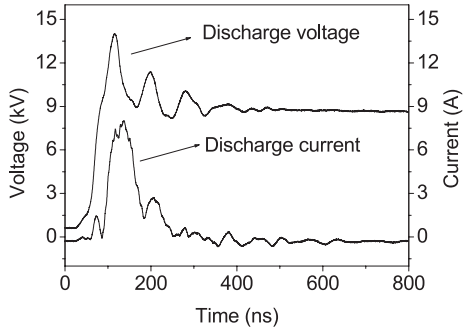

Fig. 2. Typical waveforms of discharge voltage and discharge current in N_2.

a chemical kinetic model to analyze the time evolution of the different main species involved in a flue gas initially stressed by a pulsed corona discharge and calculate the electron-molecule reaction coefficients in the flue gas. Sathiamoorthy et al. [29] developed a kinetic model to characterize the chemical reactions occurring in a pulsed streamer corona discharge.

However, little has been done about the spatially resolved measurements of the active and excited-state species in the pulsed streamer discharge. As it is well-known, spatial distribution characteristics of active species are very important to develop the kinetic model and understand the mechanism of plasma processing. The vibrational temperature is an important character of the pulsed streamer discharge and has a close relationship with the kinetics of the particles in the plasma. In this article, we present the spatially resolved spectrum diagnostic results of the emission intensity of OH ($A^2\Sigma \rightarrow X^2\Pi$, 0-0) in positive pulsed streamer plasma with a wire-plate electrode configuration, which can produce a larger plasma volume and is closer to industrial application. The effects of pulse peak voltage, pulse repetition rate and the added O_2 flow rate on the spatial distributions of the emission intensity of OH ($A^2\Sigma \rightarrow X^2\Pi$, 0-0) and the vibrational temperatures in the radial direction are investigated. This measurement plays a crucial role in understanding the discharge characters of pulsed streamer discharge and establishing the molecule reaction dynamics model of pulsed streamer discharge.

2 Experimental setup

The experimental setup is illustrated schematically in Figure 1. It is composed of a pulsed power supply, a discharge reactor, an optical detection system and a gas-mixing chamber. The power supply including charge and discharge circuit is mainly composed of a direct current high voltage unit, a pulse generator and a rotary spark gap. The pulsed power can supply high voltage pulse with a rising time of about 20 ns, a pulse width of about 60 ns, and an adjustable repetition rate in rang of 10–200 Hz. The discharge voltage is measured with an oscilloscope (Tektronix TDS3052B) and a 1:1000 high-voltage probe (Tektronix P6015A 1000×3.0 pF 100 MΩ). The discharge current is measured with a current probe (Tektronix TCP202). Figure 2 shows the waveforms of the discharge voltage and current. The discharge is generated in a stainless-steel reactor so that the environmental conditions could be controllable. The discharge reactor is evacuated with a rotary pump. In order to reduce the interferences of the discharge to the detection system and other instruments, the high-voltage pulse power supply is placed in a double shielding box. Both the pulsed power supply and the reactor are grounded separately. The wire-plate distance in the reactor is adjustable in the range of 0–30 mm. The wire-plate electrode is placed in the center of the stainless-steel reactor and the plasma is generated in the space. A stainless steel plane (56 mm × 56 mm) acts as the grounded electrode. The stainless steel wire, 48 mm long, 0.2 mm in diameter and 20 mm of wire spacing, is fixed 7 mm apart from the grounded electrode. The head of optical fiber is parallelly placed to the wire electrode and can be adjustable in the radial direction. The optical emission from the discharge region goes through a copper pipe (20 mm in length) with a slit of 1 mm into the optical fiber and is collected by a MODEL SP-305 grating monochrometer (grating groove is 1200 lines/mm, blazing wavelength is 350 nm). In order to increase signal-to-noise ratio, the inner wall of the copper pipe are painted blackly to absorb stray light and prevent unparallel light in copper pipe from entering the optical fiber. After the diffraction of the grating, the spectral light is converted into an electrical signal by a photo multiplication tube (mode R928). The signal from photo multiplication tube is transformed into number signal by the NCL (an interface between grating monochrometer and computer) and is recorded by a computer. High purity N_2 (99.999%) and high purity O_2 (99.999%) are used as discharge gases under the pressure of 1.013×10^5 Pa. The N_2 bubbles the water to control humidity in discharge reactor. The temperature of the water is heated at 100 °C. When the N_2 bubbles through the water and uniformly diffuses into the discharge space, the

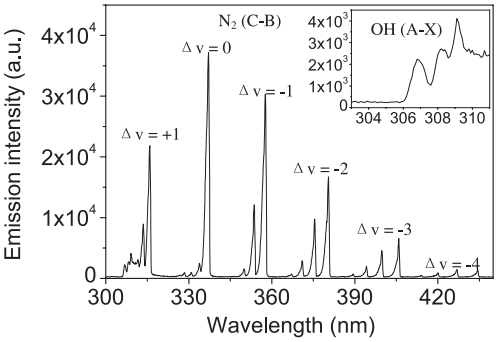

Fig. 3. Typical emission spectra of OH ($A^2\Sigma \rightarrow X^2\Pi$ 0-0) and N_2 ($C^3\Pi_u \rightarrow B^3\Pi_g$) generated by a positive pulsed streamer discharge in N_2 and H_2O mixture at 30 kV pulse peak voltage and 48 Hz pulse repetition rate.

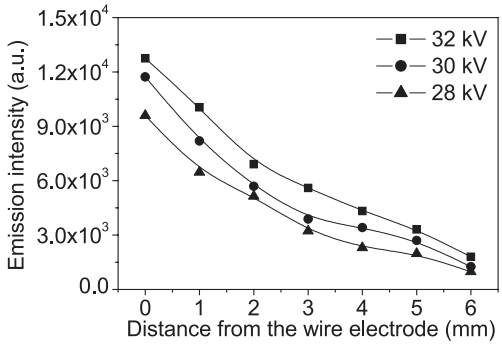

Fig. 4. The spatial distributions of the emission intensity of OH ($A^2\Sigma \rightarrow X^2\Pi$, 0-0) in the discharge gap at different pulse peak voltages and 64 Hz pulse repetition rate.

gas temperature is about 80 °C. The water vapor concentration is about 10% in discharge reactor.

3 Experimental results and discussion

3.1 The emission spectrum emitted from the high-voltage positive pulsed streamer discharge

In the positive pulsed steamer discharge at atmospheric pressure, electrons with high migration rate can be accelerated by the imposed instantaneous electric field and obtain a high kinetic energy. The non-elastic collisions between the energetic electrons and the ambient molecules will produce OH, O, H, N, HO_2, N^+ and O_2^- etc. chemically active species. Figure 3 shows a typical emission spectrum produced in a positive pulsed streamer discharge of N_2 and H_2O mixture at atmospheric pressure with 30 kV pulse peak voltage and 48 Hz pulse repetition rate. The N_2 flow rate in the reactor is kept at 200 ml/min. The emission spectrum mainly consists of OH ($A^2\Sigma \rightarrow X^2\Pi$, 0-0) and $N_2(C^3\Pi_u \rightarrow B^3\Pi_g)$.

From Figure 3, we can see that the emission spectrum of OH ($A^2\Sigma \rightarrow X^2\Pi$, 0-0) is seriously interfered by the emission spectrum of the $\Delta v = +1$ vibration transition band of N_2 ($C^3\Pi_u \rightarrow B^3\Pi_g$). Therefore, it is necessary to subtract the emission intensity of the $\Delta v = +1$ vibration transition band of N_2 ($C^3\Pi_u \rightarrow B^3\Pi_g$) from the overlapping spectra to get the emission intensity of OH ($A^2\Sigma \rightarrow X^2\Pi$, 0-0). In our previous work [30], a Gaussian form has been used for the deconvolution of the overlapping emission spectrum. The emission intensity of OH ($A^2\Sigma \rightarrow X^2\Pi$, 0-0) can be evaluated with a satisfactory accuracy.

3.2 Determination of the vibrational temperature of N_2 (C)

The vibrational temperature of N_2 (C) can be determined from the relative vibrational populations of N_2 (C). The relative vibrational populations of N_2 (C) can be determined through equation (1):

$$S_{v'v''} \propto N_{v'}(\mathrm{FC})_{v'v''} R_e^2(r_{v'v''}) v_{v'v''}^3 \quad (1)$$

where $S_{v'v''}$ is the integral emission intensity, $N_{v'}$ is the population of the electronic excitation state vibrational energy level v', $(\mathrm{FC})_{v'v''}$ is the corresponding Frank-Condon factor (quoted from Ref. [31]), $R_e(r_{v'v''})$ is electronic transition moment and $R_e(r_{v'v''})$ is nearly constant, $v_{v'v''}$ is the corresponding transition frequency. By calculating the integral emission intensity of the $\Delta v = -3$ vibration transition band of N_2 ($C^3\Pi_u \rightarrow B^3\Pi_g$), the relative vibrational populations of N_2 (C) can be determined. The vibrational temperature of N_2 (C) can be determined by the following equation:

$$N_1/N_0 = e^{-\Delta E/kT_v} \quad (2)$$

where N_1 and N_0 are the relative vibrational populations of the 1 and 0 vibrational states, respectively. ΔE is the energy difference between the 1 and 0 vibrational states and k is the Boltzman's constant. T_v stands for the vibrational temperature. Therefore, the vibrational temperature between the 1 and 0 vibrational states can be determined, and the vibrational temperatures between the 2 and 1, 3 and 2, 4 and 3 vibrational states also can be determined with the same method. Then the mean vibrational temperature of N_2(C) can be obtained.

3.3 The effects of pulse peak voltage on the spatial distributions of the emission intensity of OH ($A^2\Sigma \rightarrow X^2\Pi$, 0-0) and the vibrational temperature of N_2 (C)

The spatially resolved measurements of the emission intensity of OH ($A^2\Sigma \rightarrow X^2\Pi$, 0-0) at 28, 30 and 32 kV are presented in Figure 4. The pulse repetition rate is remained at 64 Hz and the N_2 flow rate in the reactor is kept at 200 ml/min for all measurements. It can be seen that the emission intensity of OH ($A^2\Sigma \rightarrow X^2\Pi$, 0-0) increases with increasing the pulse peak voltage at the same position and decreases with increasing the distance

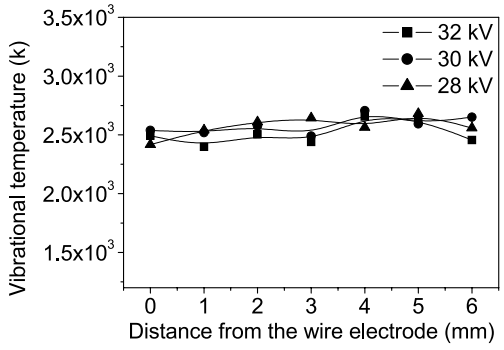

Fig. 5. The spatial distributions of the vibrational temperature of N_2 (C) in the discharge gap at different pulse peak voltages and 64 Hz pulse repetition rate.

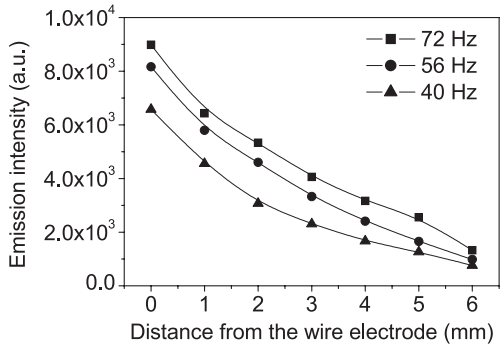

Fig. 6. The spatial distributions of the emission intensity of OH ($A^2\Sigma \rightarrow X^2\Pi$, 0-0) in the discharge gap at different pulse repetition rates and 30 kV pulse peak voltage.

from the wire electrode. Increasing the pulse peak voltage can lead to an increase of the high-energy electron density and the electron mean energy. More OH ($A^2\Sigma$) molecules can be produced. Therefore, the emission intensity of OH ($A^2\Sigma \rightarrow X^2\Pi$, 0-0) increases with increasing the pulse peak voltage. The high-energy electron density and the electron mean energy decreases with increasing the distance from the wire electrode. Then, the emission intensity of OH ($A^2\Sigma \rightarrow X^2\Pi$, 0-0) decreases with the increasing of the distance from the wire electrode.

Figure 5 shows the spatial distributions of the vibrational temperatures of N_2 (C). As can be seen, the vibrational temperatures of N_2 (C) are nearly independent of the pulse peak voltage and keep almost constant in the radial direction under the present experimental conditions. Due to the good thermal conductivity in streamer of the discharge, the vibrational temperatures of N_2 (C) keep almost constant in the radial direction.

3.4 The effects of pulse repetition rate on the spatial distributions of the emission intensity of OH ($A^2\Sigma \rightarrow X^2\Pi$, 0-0) and the vibrational temperature of N_2 (C)

Figure 6 shows the spatial distributions of the emission intensity of OH ($A^2\Sigma \rightarrow X^2\Pi$, 0-0) at 40, 56 and 72 Hz. The pulse peak voltage is kept at 30 kV and the N_2 flow rate

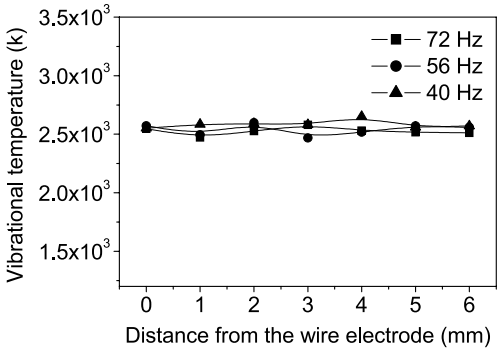

Fig. 7. The spatial distributions of the vibrational temperature of N_2 (C) in the discharge gap at different pulse repetition rates and 30 kV pulse peak voltage.

in the reactor is kept at 200 ml/min for all measurements. It shows that the emission intensity of OH ($A^2\Sigma \rightarrow X^2\Pi$, 0-0) increases with increasing the pulse repetition rate at the same position and decreases with increasing the distance from the wire electrode. Increasing the pulse repetition rate can lead to an increase in high-energy electron density proportionally, and then more OH ($A^2\Sigma$) molecules can be produced. Therefore, the emission intensity of OH ($A^2\Sigma \rightarrow X^2\Pi$, 0-0) increases with increasing the pulse repetition rate. The high-energy electron density and the electron mean energy decrease with increasing the distance from the wire electrode. Therefore, the emission intensity of OH ($A^2\Sigma \rightarrow X^2\Pi$, 0-0) decreases with increasing the distance from the wire electrode.

Figure 7 shows the spatial distributions of the vibrational temperatures of N_2 (C). It can be seen that the vibrational temperatures of N_2 (C) are nearly independent of the pulse repetition rate and keep almost constant in the radial direction under the present experimental conditions. Due to the good thermal conductivity in streamer of the discharge, the vibrational temperatures of N_2 (C) keep almost constant in the radial direction.

3.5 The effects of O_2 addition on the spatial distributions of the emission intensity of OH ($A^2\Sigma \rightarrow X^2\Pi$, 0-0) and the vibrational temperature of N_2 (C)

In order to investigate the effects of oxygen on the emission intensity of OH ($A^2\Sigma \rightarrow X^2\Pi$, 0-0) and the vibrational temperature of N_2 (C), oxygen is added into the N_2 and H_2O mixture in the positive pulsed streamer discharge. When oxygen is added, the added O_2 capture a lot of free electrons and form O_2^- ions and the humidity enhances the attachment of electrons to O_2, thus the added O_2 decrease greatly the density of free electrons and the electron mean energy in the discharge gap [20,21,32]

$$e + O_2 \rightarrow O_2^- \quad (3)$$

$$e + O_2 + M \rightarrow O_2^- + M \quad (4)$$

where M maybe N_2, O_2, and H_2O molecule.

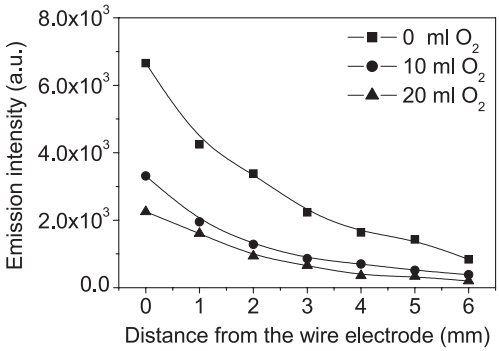

Fig. 8. The spatial distributions of the emission intensity of OH ($A^2\Sigma \rightarrow X^2\Pi$, 0-0) in the discharge gap at different oxygen flow rates, 30 kV pulse peak voltage, and 48 Hz pulse repetition rate.

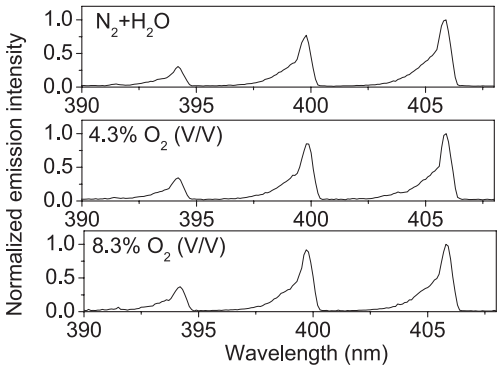

Fig. 9. The normalized emission spectra of a part of the $\Delta v = -3$ vibration transition band of N_2 ($C^3\Pi_u \rightarrow B^3\Pi_g$) (0-3, 1-4, 2-5) at 0 mm distance from the wire electrode at different oxygen flow rates, 30 kV pulse peak voltage, and 48 Hz pulse repetition rate.

Figure 8 shows the spatial distributions of the emission intensity of OH ($A^2\Sigma \rightarrow X^2\Pi$, 0-0) at oxygen flow rates of 0, 10 (4.3% O_2 (V/V)) and 20 (8.3% O_2 (V/V)) ml/min at 30 kV pulse peak voltage and 48 Hz pulse repetition rate. The N_2 flow rate in the reactor is kept at 200 ml/min for all measurements. It can be seen that the emission intensity of OH ($A^2\Sigma \rightarrow X^2\Pi$, 0-0) decreases with increasing the oxygen flow rate at the same position and decreases with the distance from the wire electrode. Increasing the flow rate of oxygen can lead to a decrease of the high-energy electron density and the electron mean energy, and then fewer OH ($A^2\Sigma$) molecules can be produced. Therefore, the emission intensity of OH ($A^2\Sigma \rightarrow X^2\Pi$, 0-0) decreases with increasing the oxygen flow rate. Because the high-energy electron density and the electron mean energy decreases with increasing of the distance from the wire electrode, the emission intensity of OH ($A^2\Sigma \rightarrow X^2\Pi$, 0-0) decreases with increasing the distance from the wire electrode.

Figure 9 shows a part of normalized emission spectra of the $\Delta v = -3$ vibration transition band of N_2 ($C^3\Pi_u \rightarrow B^3\Pi_g$) (0-3, 1-4, 2-5) at oxygen flow rates of 0, 10 (4.3% O_2 (V/V)) and 20 (8.3% O_2 (V/V)) ml/min respectively at 0 mm distance from the wire electrode. It

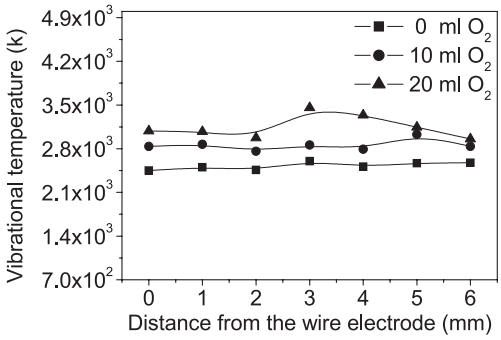

Fig. 10. The spatial distributions of the vibrational temperature of N_2 (C) in the discharge gap at different oxygen flow rates, 30 kV pulse peak voltage, and 48 Hz pulse repetition rate.

can be observed that an increase with oxygen flow rate results in characteristic changes in the emission spectrum of N_2 ($C^3\Pi_u \rightarrow B^3\Pi_g$). Brandenburg et al. [33] have found that the vibrational distribution of N_2 (C) is in contrast to the corresponding Franck-Condon factors in pure nitrogen and the added oxygen in nitrogen can result in characteristic changes in the emission spectrum of N_2 ($C^3\Pi_u \rightarrow B^3\Pi_g$). And they point out that these phenomena suggest indirect mechanisms (e.g. via N_2-metastable states) are dominating the excitation process in pure nitrogen. The structure of the emission spectrum of N_2 ($C^3\Pi_u \rightarrow B^3\Pi_g$) for higher oxygen flow rate is in better agreement with the Franck-Condon factors, thus referring to direct electronic excitation. In our present experiment, we have also observed same results.

Figure 10 shows the spatial distributions of the vibrational temperatures of N_2 (C) in the radial direction. As can be seen, the vibrational temperatures of N_2 (C) increase with increasing the oxygen flow rate at the same position and keep almost constant in the radial direction under the present experimental conditions. Because increasing the oxygen flow rate can result in characteristic changes in the emission spectrum of N_2 ($C^3\Pi_u \rightarrow B^3\Pi_g$), the vibrational temperatures of N_2 (C) increase with increasing the oxygen flow rate at the same position. Moreover, due to the good thermal conductivity in the streamer of the discharge, the vibrational temperatures of N_2 (C) keep almost constant in the radial direction.

4 Conclusions

In this paper, we have successfully recorded the emission spectrum of OH ($A^2\Sigma \rightarrow X^2\Pi$, 0-0) in the high-voltage positive pulsed streamer discharge with a wire-plate electrode configuration at atmospheric pressure. The severe electromagnetic interference caused by the pulsed streamer discharge itself has been overcome by double shielding and specially designed multiple grounded. The effects of pulse peak voltage, pulse repetition rate, and the flow rate of oxygen on the spatial distributions of the emission intensity of OH ($A^2\Sigma \rightarrow X^2\Pi$, 0-0) have

been obtained. It has been found that the emission intensity of OH ($A^2\Sigma \rightarrow X^2\Pi$, 0-0) increases with increasing the pulse peak voltage and the pulse repetition rate and decreases with increasing the distance from the wire electrode. When the different oxygen flows are added in N_2 and H_2O mixture gas, the emission intensity of OH ($A^2\Sigma \rightarrow X^2\Pi$, 0-0) decreases with increasing the oxygen flow rate. The vibrational temperature of N_2 (C) is nearly independent of pulsed peak voltage and pulsed repetition rate, but increases with increasing O_2 concentration and keeps almost constant in the radial direction under the present experimental conditions.

The author would like to thank professor Xuechu Li for friendly discussion and suggestion. This work is supported by the united fund of the National Natural Science Foundation Committee of China and Engineering Physical Institute of China granted under No. 10276008 and the fund of Liaoning Province Natural Science Foundation Committee granted under No. 20022138.

References

1. A. Mizuno, J.S. Clements, R.H. Davis, IEEE Trans. Ind. Appl. **22**, 516 (1986)
2. R.P. Dahiya, S. K. Mishra, A. Veefkind, IEEE Trans. Plasma Sci. **21**, 346 (1993)
3. A.T. Sugiarto, S. Ito, T. Ohshima, M. Sato, J.D. Skalny, J. Electrostat. **58**, 135 (2003)
4. J.J. Lowke, R. Morrow, IEEE Trans. Plasma Sci. **23**, 661 (1995)
5. A. Abou-Ghazala, S. Katsuki, K.H. Schoenbach, F.C. Dobbs, K.R. Moreira, IEEE Trans. Plasma Sci. **30**, 1449 (2002)
6. M. Yamamoto, M. Nishioka, M. Sadakata, J. Electrostat. **56**, 173 (2002)
7. T. Oda, J. Electrostat. **57**, 293 (2003)
8. U. Roland, F. Holzer, F.D. Kopinke, Catal. Today **73**, 315 (2002)
9. N.M. Šišović, G.Lj. Majstorović, N. Konjević, Eur. Phys. J. D **32**, 347 (2005)
10. W. Ebeling, H. Hache, M. Spahn, Eur. Phys. J. D **23**, 265 (2003)
11. K.P. Yan, E.J.M. van Heesch, A.J.M. Pemen, P.A.H.J. Huijbrechts, J. Electrostat. **51-52**, 218 (2001)
12. F. Liu, W.C. Wang, S. Wang, C.S. Ren, Y.N. Wang, Plasma Sci. Technol. **7**, 2851 (2005)
13. V.A. Lozovsky, I. Derzy, S. Cheskis, Chem. Phys. Lett. **284**, 407 (1998)
14. A.A. Joshi, B.R. Locke, P. Arce, W.C. Finney, J. Hazard. Mater. **41**, 3 (1995)
15. W.F.L.M. Hoeben, E.M. van Veldhuizen, W.R. Rutgers, C.A.M.G. Cramers, G.M.W. Kroesen, Plasma Sources Sci. Technol. **9**, 361 (2000)
16. B. Sun, M. Sato, A. Harano, J.S. Clements, J. Electrostat. **43**, 115 (1998)
17. S.K. Tang et al., J. Vac. Sci. Technol. A **18**, 2213 (2000)
18. W.C. Wang, F. Liu, J.L. Zhang, C.S. Ren, Spectrosc. Spect. Anal. **24**, 1288 (2004) *(in Chinese)*
19. W.C. Wang, S. Wang, F. Liu, W. Zheng, D.Z. Wang, Spectrochimica Acta A **63**, 477 (2006)
20. W.C. Wang, F. Liu, J.L. Zhang, Y.N. Wang, Spectrochimica Acta A **59**, 3267 (2003)
21. W.C. Wang, J.L. Zhang, F. Liu, Y. Liu, Y.N. Wang, Vacuum **74**, 333 (2004)
22. R. Ono, T. Oda, IEEE Trans. Ind. Appl. **37**, 709 (2001)
23. R. Ono, T. Oda, IEEE Trans. Ind. Appl. **36**, 82 (2000)
24. R. Ono, T. Oda, in *Proceedings of Thirty-Fourth IAS Annual Meeting, Industry Applications Conference, Conference Record of the 1999 IEEE* (1999), Vol. 3, p. 1461
25. R. Ono, T. Oda, J. Phys. D: Appl. Phys. **35**, 2133 (2002)
26. T. Namihira, D. Wang, S. Katsuki, R. Hackam, H. Akiyama, IEEE Trans. Plasma Sci. **31**, 1091 (2003)
27. E.M. van Veldhuizen, W.R.J. Rutgers, J. Phys. D: Appl. Phys. **35**, 2169 (2002)
28. O. Eichwald, M. Yousfi, A. Hennad, M.D. Benabdessadok, J. Appl. Phys. **82**, 4781 (1997)
29. G. Sathiamoorthy, S. Kalyana, W. C. Finney, R.J. Clark, B.R. Locke, Ind. Eng. Chem. Res. **38**, 1844 (1999)
30. F. Liu, W. Wang, W. Zheng, Y. Wang, Eur. Phys. J. D **38**, 515 (2006)
31. S.N. Suchard, *Spectroscopic Data: Heternuclear Diatomic Molecules Part B* (The Aerospace Corporation Los Angeles, California, 1975), Vol. 1
32. B.M. Penetrante, J.N. Bardsley, M.C. Hsiao, Jpn J. Appl. Phys. **36**, 5007 (1997)
33. R. Brandenburg, K.V. Kozlov, A.M. Morozov, H.E. Wagner, P. Michel, in *Proceedings of 26th Int. Conf. on Phenomena in Ionized Gases (ICPIG-26)*, Greifswald, Germany (2003), Vol. 4, p. 43